the *trans*-2 and *cis*-2 tetraols (rt 16.2 and 20.6 min, respectively)) the presence of two new peaks (minor, rt 22.2 min; and major, rt 27.7 min). These peaks, which were ascribed to the two diastereomeric triols formed upon reduction of a keto diol, accounted for ~38% of the total products derived from **2a**. The larger of these two peaks gave an ultraviolet spectrum corresponding to a 7,8,9,10-tetrahydro-BP chromophore. In a similar experiment, **1a** was allowed to react for 26 h ($\sim 2 \times t_{1/2}$) at pH 8.2, acidified, and then treated with excess sodium borohydride. Chromatography of the resultant mixture indicated that no triols were present. Under similar conditions (overnight incubation at pH 7.9), the keto diol formed from **2a** was completely lost, as demonstrated by the inability to detect triols by borohydride trapping subsequent to this incubation.

Charge Separation in Carotenoporphyrin-Quinone Triads: Synthetic, Conformational, and Fluorescence Lifetime Studies

Devens Gust,*[†,#] Thomas A. Moore,*[†] Paul A. Liddell,[†] Gregory A. Nemeth,[†] Lewis R. Makings,[†] Ana L. Moore,[†] Donna Barrett,[†] Peter J. Pessiki,[†] René V. Bensasson,[#] Michel Rougée,[#] Claude Chachaty,[‡] F. C. De Schryver,[⊥] M. Van der Auweraer,[⊥] Alfred R. Holzwarth,[§] and John S. Connolly[±]

Contribution from the Department of Chemistry, Arizona State University, Tempe, Arizona 85287, the Laboratoire de Biophysique, ERA 951 du CNRS, Muséum National d'Histoire Naturelle, 75005 Paris, France, the Dépertement de Physico-Chimie, Centre d'Etudes Nucléaires de Saclay, 91191 Gif-sur-Yvette Cedex, France, the Afdeling Organische Scheikunde, Katholieke Universiteit Leuven, Celestijnenlaan 200F, Leuven, Belgium, the Max Planck Institute fur Strahlenchemie, Mulheim, West Germany, and the Photoconversion Research Branch, Solar Energy Research Institute, Golden, Colorado 80401. *Received February 25, 1986*

Abstract: Carotenoid-porphyrin-quinone triad molecules undergo a photodriven two-step electron-transfer reaction which results in the generation of a high-energy charge-separated state with a lifetime on the microsecond time scale at ambient temperatures in fluid solution. These systems mimic the initial charge separation steps of photosynthesis. A series of these tripartite molecules which differ systematically in the nature of the linkages joining the porphyrin to the quinone and carotenoid moieties has been synthesized in order to investigate the effect of structure on the yield and lifetime of the charge-separated state. The time-averaged solution conformations of these molecules have been determined from porphyrin ring current induced shifts in the ^{1}H NMR resonances of the carotenoid and quinone moieties. Studies of the triads and related molecules in dichloromethane solution using time-correlated single photon counting fluorescence lifetime techniques have yielded the rate constant for the first of the photoinitiated electron-transfer steps as a function of the linkage joining the porphyrin and the quinone. The rate constants range from 1.5×10^8 to 9.7×10^9 s^{-1}. For most members of the series, the results are consistent with an exponential dependence of the electron-transfer rate on the experimentally determined donor-acceptor separation, with the exponential factor $\alpha = 0.6$ Å^{-1}.

Molecular triads, consisting of porphyrins covalently linked to both carotenoid polyenes and quinones, and related systems have been developed as models for photosynthetic charge separation, singlet energy transfer (antenna function), and triplet energy transfer (photoprotection from singlet oxygen via carotenoid quenching of the chlorophyll triplet state).[1-11] With respect to charge separation, triad molecules such as **1**, in common with porphyrin-quinone dyad molecules,[12] carry out photodriven electron transfer in good yield. In addition, the triads produce energetic charge-separated states with lifetimes on the microsecond time scale.[6-8,10,11] The key to long lifetimes in these systems is a biomimetic two-step intramolecular electron transfer (see Scheme I). Excitation of the porphyrin moiety (step 1) yields the porphyrin first excited singlet state C-^{1}P-Q, which donates an electron to the quinone to produce an initial charge-separated state C-P$^{\bullet+}$-Q$^{\bullet-}$ (step 2). This state has two possible pathways for decay. Charge recombination (step 3) is a facile reaction which yields the ground state. Such back-electron-transfer reactions are to be avoided in photosynthesis or other energy conserving systems because they degrade the chemical potential stored in the charge-separated state to heat. In the triads, a second electron-transfer reaction (step 4) competes with step 3 to yield a final charge-separated state C$^{\bullet+}$-P-Q$^{\bullet-}$. This state lives from hundreds

Scheme I

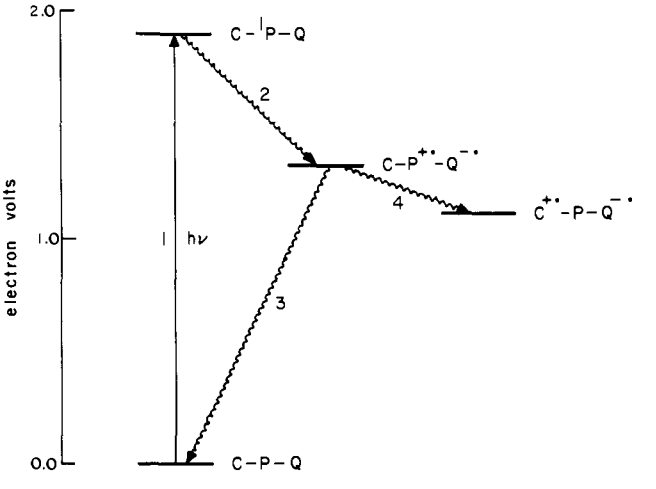

[†] Arizona State University.
[#] Muséum National d'Histoire Naturelle.
[‡] Département de Physico-Chimie, CEN Saclay.
[⊥] Katholieke Universiteit Leuven.
[§] Max Planck Institute.
[±] Solar Energy Research Institute.

(1) Dirks, G.; Moore, A. L.; Moore, T. A.; Gust, D. *Photochem. Photobiol.* **1980**, *32*, 277-280.
(2) Moore, A. L.; Dirks, G.; Gust, D.; Moore, T. A. *Photochem. Photobiol.* **1980**, *32*, 691-695.

0002-7863/87/1509-0846$01.50/0

of nanoseconds to microseconds (depending upon the solvent) before ultimately returning to the ground state and can be readily detected by observation of the strong carotenoid radical cation absorption in the 950-nm region. A lifetime on the microsecond time scale is long enough to allow harvesting of the potential energy stored in the charge-separated state by reaction with other species in solution or at a phase boundary.[11] Recently, the generality of this approach to stabilization of a charge-separated state has been demonstrated by the preparation and study of a different porphyrin–quinone triad species.[13]

In order to elucidate the physical and chemical factors controlling charge separation and recombination in the triads, one would ideally like to be able to determine independently the kinetics of each step in the scheme and to study the influence of electronic and structural factors on the reaction rates. For any particular combination of electron donors and acceptors, these rates are expected to be critically dependent on the degree of orbital overlap and therefore on the relative separation and orientation of the donor and acceptor moieties. These factors are in turn governed by the nature of the covalent linkages joining these moieties. We report here the synthesis of triads **1–7**, which have been prepared as model systems for the investigation of these factors. Porphyrin–quinone analogues of the triads, **8–11**, have also been synthesized.

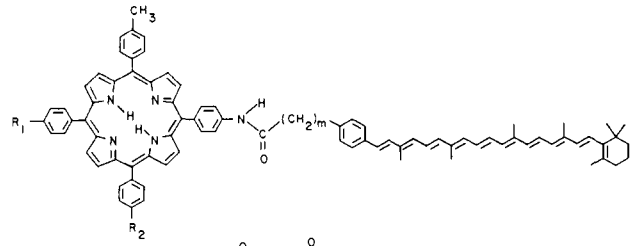

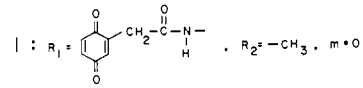

1 : R_1 = , R_2 = $-CH_3$, m = 0

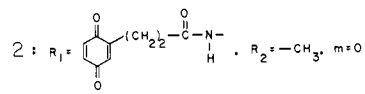

2 : R_1 = , R_2 = $-CH_3$, m = 0

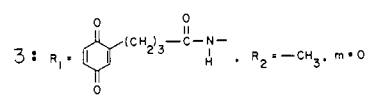

3 : R_1 = , R_2 = $-CH_3$, m = 0

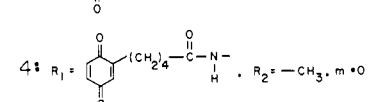

4 : R_1 = , R_2 = $-CH_3$, m = 0

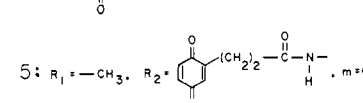

5 : R_1 = $-CH_3$, R_2 = , m = 0

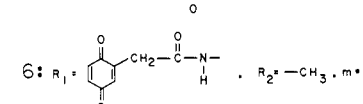

6 : R_1 = , R_2 = $-CH_3$, m = 1

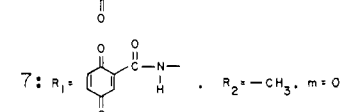

7 : R_1 = , R_2 = $-CH_3$, m = 0

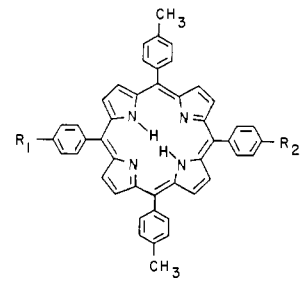

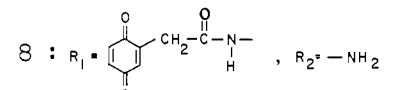

8 : R_1 = , R_2 = $-NH_2$

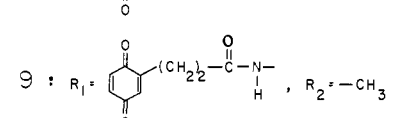

9 : R_1 = , R_2 = $-CH_3$

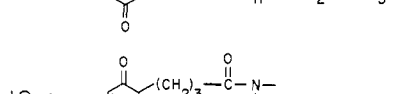

10 : R_1 = , R_2 = $-NH_2$

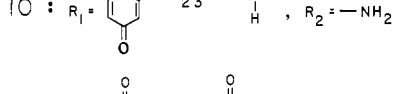

11 : R_1 = , R_2 = $-NH_2$

In addition, a meaningful study of the dependence of electron-transfer rate on structural factors requires an independent determination of molecular conformation. We have therefore elucidated the time-averaged solution conformations of **1–6** and **8–11** by analyzing the porphyrin aromatic ring current induced shifts in the ^1H NMR resonances of the carotenoid and quinone moieties.

Finally, the rate of the initial charge separation (step 2) in these

(3) Bensasson, R. V.; Land, E. J.; Moore, A. L.; Crouch, R. L.; Dirks, G.; Moore, T. A.; Gust, D. *Nature (London)* **1981**, *290*, 329–332.

(4) Gust, D.; Moore, A. L.; Joy, A.; Tom, R.; Moore, T. A.; Bensasson, R. V.; Land, E. J. *Science (Washington, D.C.)* **1982**, *216*, 982–984.

(5) Liddell, P. A.; Nemeth, G. A.; Lehman, W. R.; Joy, A. M.; Moore, A. L.; Bensasson, R. V.; Moore, T. A.; Gust, D. *Photochem. Photobiol.* **1982**, *36*, 641–645.

(6) Gust, D.; Mathis, P.; Moore, A. L.; Liddell, P. A.; Nemeth, G. A.; Lehman, W. R.; Moore, T. A.; Bensasson, R. V.; Land, E. J.; Chachaty, C. *Photochem. Photobiol.* **1983**, *37S*, S46.

(7) Moore, T. A.; Mathis, P.; Gust, D.; Moore, A. L.; Liddell, P. A.; Nemeth, G. A.; Lehman, W. R.; Bensasson, R. V.; Land, E. J.; Chachaty, C. In *Advances in Photosynthesis Research*; Sybesma, C., Ed.; Nijhoff/Junk: The Hague, 1984; pp 729–732.

(8) Moore, T. A.; Gust, D.; Mathis, P.; Mialocq, J. C.; Chachaty, C.; Bensasson, R. V.; Land, E. J.; Diozi, D.; Liddell, P. A.; Nemeth, G. A.; Moore, A. L. *Nature (London)* **1984**, *307*, 630–632.

(9) Gust, D.; Moore, T. A.; Bensasson, R. V.; Mathis, P.; Land, E. J.; Chachaty, C.; Moore, A. L.; Liddell, P. A.; Nemeth, G. A. *J. Am. Chem. Soc.* **1985**, *107*, 3631–3640.

(10) Gust, D.; Moore, T. A. *J. Photochem.* **1985**, *29*, 173–184.

(11) Seta, P.; Bienvenue, E.; Moore, A. L.; Mathis, P.; Bensasson, R. V.; Liddell, P. A.; Pessiki, P. J.; Joy, A.; Moore, T. A.; Gust, D. *Nature (London)* **1985**, *316*, 653–655.

(12) Kong, J. L.; Loach, P. A. In *Frontiers of Biological Energetics: From Electrons to Tissues*; Dutton, P. L., Leigh, J. S., Scarpa, A., Eds.; Academic: New York, 1978; pp 73–82. (b) Tabushi, I.; Koga, N.; Yanagita, M. *Tetrahedron Lett.* **1979**, *257*–260. (c) Dalton, J.; Milgrom, L. R. *J. Chem. Soc., Chem. Commun.* **1979**, 609–610. (d) Kong, J. L. Y.; Loach, P. A. *J. Heterocycl. Chem.* **1980**, *17*, 737–744. (e) Ho, T.-F.; McIntosh, A. R.; Bolton, J. R. *Nature (London)* **1980**, *286*, 254–256. (f) Ganesh, K. N.; Sanders, J. K. M. *J. Chem. Soc., Chem. Commun.* **1980**, 1129–1131. (g) Harriman, A.; Hosie, R. J. *J. Photochem.* **1981**, *15*, 163–167. (h) Netzel, T. L.; Bergkamp, M. A.; Chang, C. K.; Dalton, J. *J. Photochem.* **1981**, *15*, 451–460. (i) Nishitani, S.; Kurata, N.; Sakata, Y.; Misumi, S.; Migita, M.; Okada, T.; Mataga, N. *Tetrahedron Lett.* **1981**, 2099–2102. (j) Migita, M.; Okada, T.; Mataga, N.; Nishitani, S.; Kurata, N.; Sakata, Y.; Misumi, S. *Chem. Phys. Lett.* **1981**, *84*, 263–266. (k) Kong, J. L. Y.; Spears, K. G.; Loach, P. A. *Photochem. Photobiol.* **1982**, *35*, 545–553. (l) Ganesh, K. N.; Sanders, J. K. M. *J. Chem. Soc., Perkin Trans. 1* **1982**, 1611–1615. (m) Ganesh, K. N.; Sanders, J. K. M.; Waterton, J. C. *J. Chem. Soc., Perkin Trans. 1* **1982**, 1617–1624. (n) Bergkamp, M. A.; Dalton, J.; Netzel, T. L. *J. Am. Chem. Soc.* **1982**, *104*, 253–259. (o) Lindsey, J. S.; Mauzerall, D. C. *J. Am. Chem. Soc.* **1982**, *104*, 4498–4500. (p) Lindsey, J. S.; Mauzerall, D. C. *J. Am. Chem. Soc.* **1983**, *105*, 6528–6529. (q) McIntosh, A. R.; Siemiarczuk, A.; Bolton, J. R.; Stillman, M. J.; Ho, T.-F.; Weedon, A. C. *J. Am. Chem. Soc.* **1983**, *105*, 7215–7223. (r) Siemiarczuk, A.; McIntosh, A. R.; Ho, T.-F.; Stillman, M. J.; Roach, K. J.; Weedon, A. C.; Bolton, J. R.; Connolly, J. S. *J. Am. Chem. Soc.* **1983**, *105*, 7224–7230. (s) Nishitani, S.; Kurata, N.; Sakata, Y.; Misumi, S.; Karen, A.; Okada, T.; Mataga, N. *J. Am. Chem. Soc.* **1983**, *105*, 7771–7772. (t) Joran, A. D.; Leland, B. A.; Geller, G. G.; Hopfield, J. J.; Dervan, P. B. *J. Am. Chem. Soc.* **1984**, *106*, 6090–6092. (u) Wasielewski, M. R.; Niemczyk, M. P.; Svec, W. A.; Pewitt, E. B. *J. Am. Chem. Soc.* **1985**, *107*, 1080–1082 and references cited therein.

(13) Wasielewski, M. R.; Niemczyk, M. P.; Svec, W. A.; Pewitt, E. B. *J. Am. Chem. Soc.* **1985**, *107*, 5562–5563.

molecules has been determined by monitoring the fluorescence decay of the porphyrin singlet as a function of time. The rationale for this approach is as follows. The experimentally determined decay time τ_f of the porphyrin first excited singlet state of **1**, for example, is the reciprocal of the sum of the rates for deactivation of this state by electron transfer, fluorescence, intersystem crossing, and internal conversion. A hypothetical model system for **1** which does not undergo electron transfer to the quinone but is otherwise identical would have a longer fluorescence lifetime τ_0. Assuming irreversible electron transfer, the rate constant for charge separation k_{et} (step 2 in the scheme) would then be given by eq 1. In

$$k_{et} = (1/\tau_f) - (1/\tau_0) \quad (1)$$

the absence of such hypothetical model systems, molecules such as the hydroquinone form of a triad or of a porphyrin–quinone species should be a good approximation. Thus, a comparison of the fluorescence lifetimes of triads and porphyrin–quinones with those of the corresponding model systems allows calculation of the relevant electron-transfer rates.

Experimental Section

Synthesis and NMR Studies. The ^{1}H NMR spectra were obtained on a Bruker WM-500, AM-400, or WH-90 spectrometer or on a Varian XL-100 spectrometer and refer to ca. 1% solutions in chloroform-*d* unless otherwise specified. Chemical shifts listed in the tables are not repeated in the synthetic section. Mass spectra of the triad quinones, hydroquinones, or hydroquinone diacetates were obtained in the FAB mode at the Middle Atlantic Mass Spectrometry Laboratory. Other mass spectra were obtained on a Varian MAT 311. Elemental analyses were performed by MicAnal Laboratories, Tucson, AZ. The general outlines of the synthetic schemes employed are given in the Results section. The descriptions of the synthetic steps are given as supplementary material.

Fluorescence Decay Measurements. Unless otherwise specified, the fluorescence decay measurements were made on ca. 1×10^{-5} M solutions in dichloromethane (5- or 10-mm path length) at ambient temperatures. The samples were purified by thin-layer chromatography immediately before use. The solvent was stored over anhydrous potassium carbonate to remove any traces of hydrochloric acid.

All fluorescence decay measurements were made by the time-correlated single photon counting method. Fluorescence decays containing only components with decay times longer than ca. 1 ns were measured by using a flash lamp for excitation at 337 nm. Many of these measurements employed an Edinburgh Instruments 199 fluorescence spectrometer equipped with a 2254B photomultiplier tube. Others were conducted with a Photochemical Research Associates Model 3000 nanosecond lifetime fluorometer which was specially adapted for detection of the fluorescence of porphyrinic macrocycles[14,15] and porphyrin–quinone systems.[16] The porphyrin fluorescence emission maximum in the triads is ca. 655 nm. In order to increase the signal-to-noise ratio, the emission monochromator was usually replaced with a long pass filter (570 or 640 nm). Fluorescence profiles containing components with decay times less than 1 ns were measured with excitation at 590 nm by using a synchronously pumped, mode-locked, cavity-dumped dye laser as the excitation source. The experimental details are described elsewhere.[17,18]

The observed fluorescence decay obtained as described above is the convolution integral of the true fluorescence decay $f(t)$ following δ excitation and an instrumental response function $I(\lambda_{ex}, \lambda_{em}, t)$. The function $f(t)$ is presumed to be of the form given in eq 2 for n = 1, 2, or 3 decays.

$$f(t) = \sum_{i=1}^{n} A_i \exp(-t/\tau_i) \quad (2)$$

The A_i and τ_i are calculated by a nonlinear least-squares curve fitting process. Goodness of fit is determined by the usual inspection of plots of the residuals and their autocorrelation functions. In addition to these qualitative criteria, χ^2, Z_{χ^2}, the runs test, and the Durbin–Watson parameters are used as quantitative criteria.

Scheme II

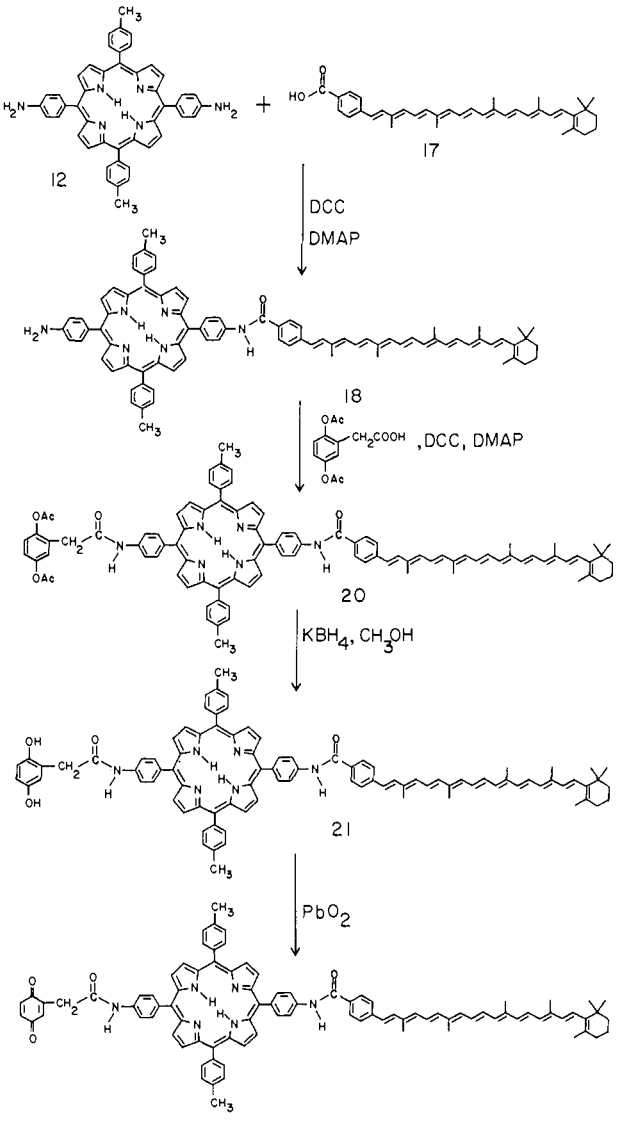

Results

Synthesis. The preparation of **1** is outlined in Scheme II. The 5,15-bis(4-aminophenyl)-10,20-bis(4-methylphenyl)porphyrin (**12**) had previously been prepared via reduction of the corresponding nitroporphyrin.[8] A superior method of preparation is to carry out the Rothemund reaction[19,20] with pyrrole, *p*-tolualdehyde, and extremely pure 4-acetamidobenzaldehyde (use of impure material results in a rather violent decomposition reaction). This produces a mixture of crystalline porphyrins from which 5,15-bis(4-acetamidophenyl)-10,20-bis(4-methylphenyl)porphyrin (**14**) may be separated by chromatography. Hydrolysis of the amide linkages yields **12** (see Experimental Section). The amide linkage between **12** and 4-(β-apo-7′-carotenyl)benzoic acid (**17**)[9] was formed by using dicyclohexylcarbodiimide and 4-(dimethylamino)pyridine. These same reagents were used to couple the resulting carotenoporphyrin **18** with (2,5-diacetoxyphenyl)acetic acid to yield the protected hydroquinone **20**. Deacetylation of **20** with potassium borohydride in methanol/dichloromethane to yield **21** followed by oxidation with lead dioxide gave **1**. Analogous synthetic routes were employed for the preparation of **6** and **7** (see Experimental Section).

A synthetic sequence similar to that in Scheme II could not be used for triads **2**–**5** because the corresponding hydroquinone derivatives with carboxylic acid side chains readily formed lactones. Therefore, a second reaction sequence was developed, as shown

(14) Connolly, J. S.; Janzen, A. F.; Samuel, E. B. *Photochem. Photobiol.* **1982**, *36*, 559–563.
(15) Connolly, J. S.; Samuel, E. B.; Janzen, A. F. *Photochem. Photobiol.* **1982**, *36*, 565–574.
(16) Siemiarczuk, A.; McIntosh, A. R.; Ho, T.-F.; Stillman, M. J.; Roach, K. J.; Weedon, A. C.; Bolton, J. R.; Connolly, J. S. *J. Am. Chem. Soc.* **1983**, *105*, 7224–7230.
(17) Boens, N.; Van den Zegel, M.; De Schryver, F. C. *Chem. Phys. Lett.* **1984**, *111*, 340–346.
(18) Holzwarth, A. R.; Wendler, J.; Wehrmeyer, W. *Photochem. Photobiol.* **1982**, *36*, 479–487.
(19) Rothemund, P. *J. Am. Chem. Soc.* **1939**, *61*, 2912.
(20) Rothemund, P.; Menotti, A. *J. Am. Chem. Soc.* **1941**, *63*, 267.

Scheme III

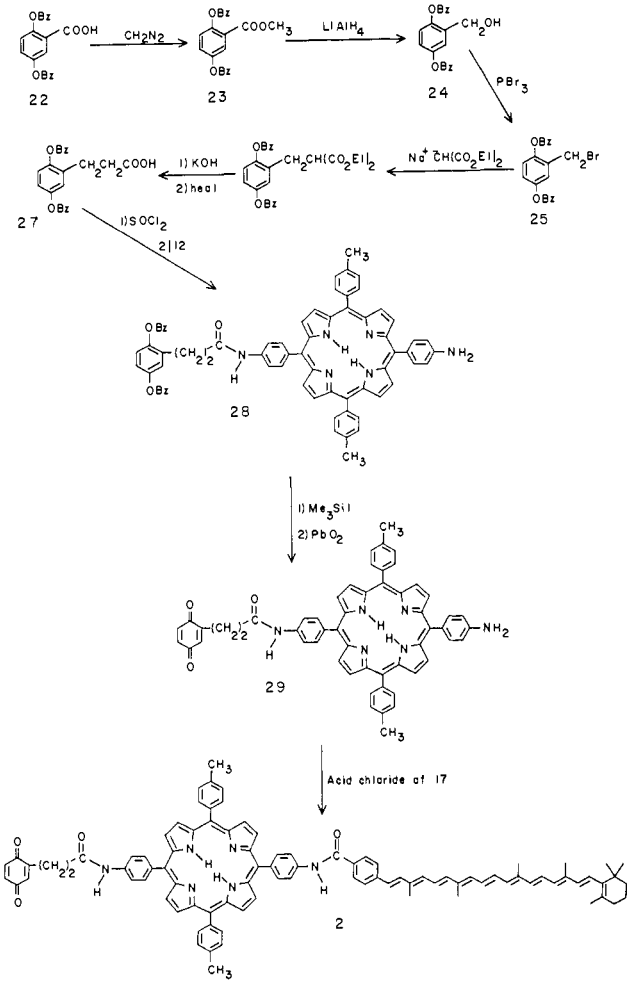

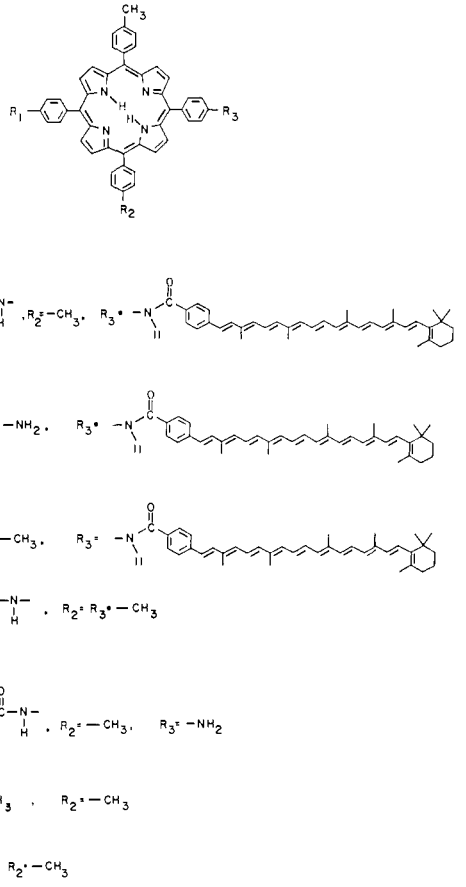

for triad **2** in Scheme III. Conversion of 2,5-bis(benzyloxy)-benzoic acid (**22**) to the methyl ester (**23**) with diazomethane was followed by reduction to the benzyl alcohol **24**. Bromination of **24** with phosphorus tribromide gave benzyl bromide **25** which was converted to 3-(2,5-bis(benzyloxy)phenyl)propanoic acid (**27**) by using the malonic ester synthesis. This acid was converted to the acid chloride and the acid chloride allowed to react with **12** to yield amide **28**. Removal of the benzyl protecting groups with iodotrimethylsilane followed by oxidation of the resulting hydroquinone with lead dioxide gave **29**, which was allowed to react with the acid chloride of **17** to yield triad **2** directly in the quinone form. Triads **3**, **4**, and **5** were prepared in an analogous fashion. The necessary protected hydroquinone precursors were prepared from **27** by conversion to the methyl ester, reduction, conversion to the chloride, and chain extension via either cyanide substitution or the malonic ester route. The 5,10-bis(4-aminophenyl)-15,20-bis(4-methylphenyl)porphyrin (**13**) required for the preparation of **5** was obtained as a coproduct from the synthesis of **12** and could be distinguished from **12** on the basis of its ^{1}H NMR spectrum.

Method of Conformational Analysis. As mentioned above, relating the photophysical behavior of the triad molecules to structural parameters requires an independent probe of molecular conformation. Simple inspection of molecular models cannot in general provide this information because the molecules could in principle assume one or more of a number of chemically reasonable conformations. This is especially true for triads **2**, **3**, **4**, and **5**, which feature chains of methylene groups. Each of the bonds joining these groups is the axis of a 3-fold rotor which undoubtedly has a relatively low energy barrier to rotation. Fortunately, ^{1}H NMR studies can provide fairly precise structural data for these molecules. Immersion of the porphyrin ring system in the magnetic field of an NMR spectrometer gives rise to large aromatic ring currents, which may be thought of as a circulation of π-electrons in a plane parallel to that of the porphyrin ring. These circulating electrons produce a local magnetic field that opposes the external field. Thus, a proton in the region of the porphyrin ring will experience the sum of the spectrometer field and the local ring current field and will have its resonance position shifted accordingly. These shifts can be quite large (up to several parts per million). The porphyrin ring current induced shift for a carotenoid or quinone proton is therefore a sensitive function of the spatial relationship of that proton to the porphyrin macrocycle.

Several theoretical and experimental approaches to the quantitative evaluation of the porphyrin ring current have appeared.[21-27] We recently adapted the ring current model of Abraham and co-workers[26,27] for the computer-assisted conformational analysis of carotenoporphyrins.[28] The same method may be used to determine the time-averaged solution conformations of **1–6** and their analogues **8–11**. The first step in such an analysis is the determination of the ring current induced resonance shifts ($\Delta\delta$) for carotenoid and quinone protons from the spectral assignments for the triads and appropriate model compounds. The porphyrin ring current model is then used to determine the molecular conformations consistent with these shifts.

Spectral Assignments. The ^{1}H NMR spectra of triads **1–6** and analogues **8–11** were obtained at 400 or 500 MHz. Lower magnetic field strengths resulted in severe overlap of resonances,

(21) Scheer, H.; Katz, J. J. In *Porphyrins and Metalloporphyrins*; Smith, K. M., Ed.; Elsevier: Amsterdam, 1975; p 399.
(22) Becker, E. D.; Bradley, R. B. *J. Chem. Phys.* **1959**, *31*, 1413.
(23) Abraham, R. J. *Mol. Phys.* **1961**, *4*, 145.
(24) Janson, T. R.; Kane, A. R.; Sullivan, J. F.; Knox, K.; Kenney, M. E. *J. Am. Chem. Soc.* **1969**, *91*, 5210.
(25) Shulman, R. G.; Wüthrich, K.; Yamane, T.; Patel, D. J.; Blumberg, W. E. *J. Mol. Biol.* **1970**, *53*, 143-157.
(26) Abraham, R. J.; Fell, S. C. M.; Smith, K. M. *Org. Magn. Reson.* **1977**, *9*, 367-373.
(27) Abraham, R. J.; Bedford, G. R.; McNeillie, D.; Wright, B. *Org. Magn. Reson.* **1980**, *14*, 418-425.
(28) Chachaty, C.; Gust, D.; Moore, T. A.; Nemeth, G. A.; Liddell, P. A.; Moore, A. L. *Org. Magn. Reson.* **1984**, *22*, 39-46.

Table I. ^{1}H NMR Chemical Shifts of Carotenoporphyrin–Quinone Triads[a,b]

	compound					
proton	**1**	**2**	**3**	**4**	**5**	**6**
C2	1.47	1.47	1.48	1.48	1.47	1.47
C3	1.62	1.62	1.62	1.62	1.62	1.63
C4	2.04	2.01	2.04	2.04	2.04	2.02
C7	6.182	6.208	6.184	6.182	6.183	6.177
C8	6.144	6.128	6.146	6.144	6.145	6.138
C10	6.163	6.168	6.165	6.163	6.164	6.158
C11	6.6–6.8	6.6–6.8	6.6–6.8	6.6–6.8	6.6–6.8	6.6–6.8
C12	6.368	6.369	6.369	6.369	6.369	6.357
C14	6.273	6.273	6.273	6.273	6.274	6.258
C15	6.6–6.8	6.6–6.8	6.6–6.8	6.6–6.8	6.6–6.8	6.6–6.8
C15′	6.6–6.8	6.6–6.8	6.6–6.8	6.6–6.8	6.6–6.8	6.6–6.8
C14′	6.341	6.335	6.333	6.337	6.335	6.328
C12′	6.486	6.477	6.479	6.483	6.483	6.441
C11′	6.6–6.8	6.6–6.8	6.6–6.8	6.6–6.8	6.6–6.8	6.6–6.8
C10′	6.450	6.442	6.442	6.446	6.446	6.388
C8′	6.67	6.66	6.658	6.65	6.66	6.639
C7′	7.068	7.056	7.058	7.064	7.062	6.975
C1′, C5′	7.629	7.609	7.614	7.623	7.619	7.561
C2′, C4′	7.997	7.978	7.984	7.991	7.988	7.436
C16, C17	1.033	1.037	1.036	1.035	1.035	1.032
C18	1.724	1.726	1.726	1.730	1.725	1.717
C19	1.983	1.985	1.985	1.985	1.984	1.982
C19′	2.102	2.095	2.096	2.099	2.099	2.078
C20	1.997	1.997	1.998	1.998	1.997	1.974
C20′	2.014	2.011	2.012	2.013	2.013	1.994
C21						3.905
P2	8.864	8.860	8.867	8.865	8.8–8.9	8.8–8.9
P3	8.821	8.828	8.846	8.843	8.8–8.9	8.8–8.9
P7	8.821	8.828	8.846	8.843	8.8–8.9	8.8–8.9
P8	8.864	8.860	8.867	8.865	8.8–8.9	8.8–8.9
P12	8.881	8.876	8.878	8.880	8.8–8.9	8.8–8.9
P13	8.881	8.876	8.878	8.880	8.8–8.9	8.8–8.9
P17	8.881	8.876	8.878	8.880	8.8–8.9	8.8–8.9
P18	8.881	8.876	8.878	8.880	8.8–8.9	8.8–8.9
5Ar2,6	8.18	8.15	8.17	8.17	8.16	8.124
5Ar3,5	7.90	7.85	7.91	7.90	7.87	7.810
10Ar2,6	8.09	8.08	8.09	8.09	8.21	8.071
10Ar3,5	7.56	7.54	7.55	7.55	8.04	7.558
10ArCH$_3$	2.709	2.70	2.703	2.707		2.699
15Ar2,6	8.23	8.22	8.22	8.22	8.09	8.162
15Ar3,5	8.06	7.98	8.04	8.05	7.55	7.885
15ArCH$_3$					2.705	
20Ar2,6	8.09	8.08	8.09	8.09	8.09	8.071
20Ar3,5	7.56	7.54	7.55	7.55	7.55	7.558
20ArCH$_3$	2.709	2.70	2.703	2.707	2.705	2.699
Q3	7.004	6.76	6.697	6.660	6.774	6.995
Q5	6.871	6.77	6.760	6.752	6.781	6.867
Q6	6.944	6.83	6.816	6.800	6.836	6.932
Q7	3.686	2.97	2.633	2.564	2.987	3.677
Q8		2.76	2.085	1.730	2.787	
Q9			2.592	1.949		
Q10				2.584		

[a] Whenever possible, chemical shifts are reported to the nearest 0.001 ppm. Although the absolute accuracy of the measurement is probably not this good, the reported values reflect the relative peak positions and separations and therefore allow assignments of closely spaced resonances. [b] See Figure 1 for numbering system. The prefix letter signifies the carotenoid (C), porphyrin (P), or quinone (Q) moiety.

especially in the carotenoid vinylic proton region, which precluded assignments. The resonances were assigned by comparisons with model compounds, single-frequency proton decoupling experiments, and COSY homonuclear shift-correlated 2-D experiments. The numbering system used to identify the protons on the various molecular fragments is shown in Figure 1. The resonance assignments for the triads are given in Table I. Similar assignments were made for porphyrin–quinone systems **8**–**11**. These assignments appear in the supplementary material.

Ideally, the model compounds used for the calculation of $\Delta\delta$ values should include all structural features present in the triad itself except for the porphyrin ring current. Such model compounds, of course, cannot exist. For the carotenoid portion of **1**–**5**

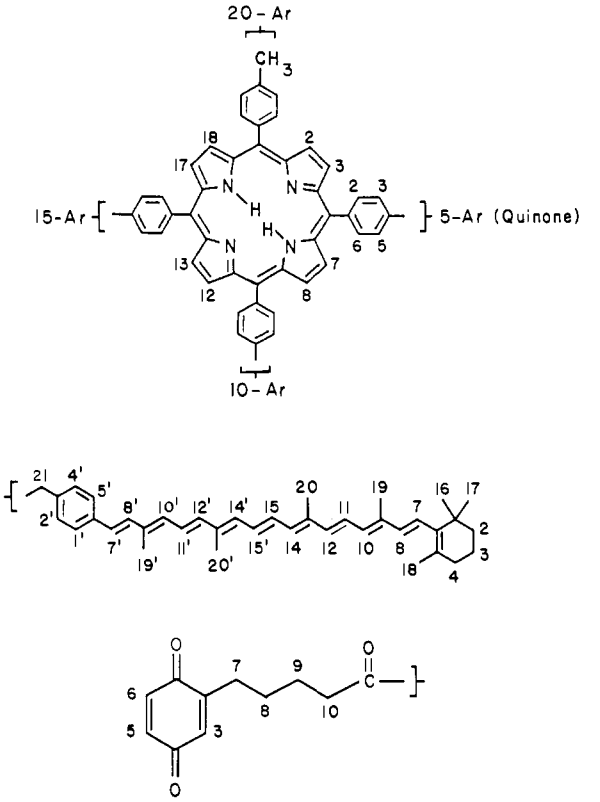

Figure 1. Numbering system used for chemical shifts (Tables I and II).

Table II. ^{1}H NMR Chemical Shifts of Model Compounds[a,b]

	carotenoids			carotenoids	
proton	**50**	**45**	proton	**50**	**45**
C2	1.47	1.46	C11	6.6–6.7	6.6–6.7
C3	1.62	1.61	C10′	6.407	6.357
C4	2.02	2.02	C8′	6.603	6.557
C7	6.178	6.179	C7′	7.000	6.877
C8	6.138	6.130	C1′,5′	7.530	7.387
C10	6.158	6.154	C2′,4′	7.829	7.228
C11	6.6–6.7	6.9–6.7	C16,17	1.031	1.030
C12	6.360	6.332	C18	1.721	1.720
C14	6.262	6.256	C19	1.995	1.984
C15	6.6–6.7	6.6–6.7	C19′	2.063	2.038
C15′	6.6–6.7	6.6–6.7	C20	1.988	1.984
C14′	6.319	6.291	C20′	1.979	1.976
C12′	6.459	6.387	C21		3.615

	quinones				
proton	**53**	**57**	**59**	**60**	**61**
Q3	7.704	6.802	6.64	6.604	6.582
Q5	6.883	6.778	~6.74	6.723	6.718
Q6	7.844	6.815	~6.76	6.761	6.752
Q7		3.310	2.79	2.484	2.452
Q8			2.48	1.871	1.580
Q9				2.294	1.721
Q10					2.268

[a] Whenever possible, chemical shifts are reported to the nearest 0.001 ppm. Although the absolute accuracy of the measurement is probably not this good, the reported values reflect the relative peak positions and separations and therefore allow assignments of closely spaced resonances. [b] See Figure 1 for numbering system. The prefix letter signifies the carotenoid (C) or quinone (Q) moiety.

both the simple amide and the aniline amide (**50**) of carotenoic acid (**17**) were investigated for use as models. The aniline amide gave better results and was used for the calculations. As an amide model for the carotenoid in **6** was not available, the corresponding methyl ester of the carotenoic acid (**45**) was employed. The model compounds for the quinone portions of the triads **1**–**5** were the corresponding simple amides of the quinone acids (**57**, **59**, **60**, and **61**). The chemical shifts of the protons in the model compounds are given in Table II.

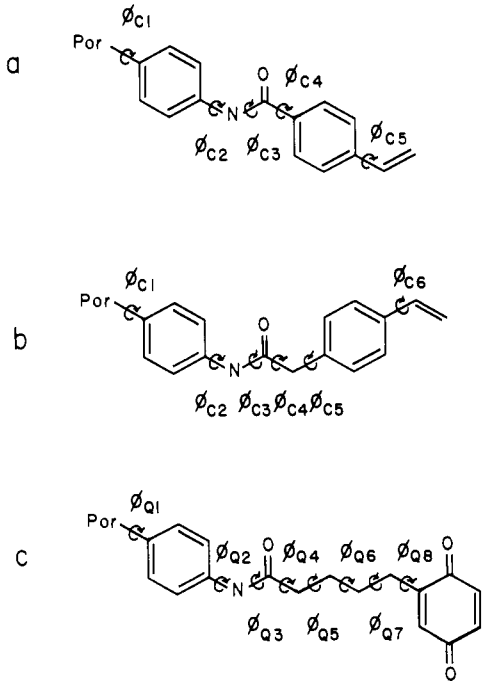

Figure 2. Numbering system used for dihedral angles (Table IV). Conventions for defining the dihedral angles are described in the text.

The porphyrin ring current induced resonance shifts ($\Delta\delta$) for the carotenoid and quinone protons were calculated by subtracting the observed chemical shift of a given proton in the model compound from that of the corresponding proton in the triad or dyad. Thus, negative $\Delta\delta$ values signify an upfield shift of the resonance (shielding). The $\Delta\delta$ values for the protons used in the conformational calculations are given in Table III.

Molecular Conformations. The method used for the calculation of molecular conformation from the ring current induced shifts has been discussed previously.[28] Briefly, the single-dipole treatment of Abraham and co-workers[26,27] approximates the contribution of the porphyrin macrocycle as the sum of the contributions of eight smaller current loops. Each of these loops is then replaced by an equivalent dipole centered in one of the four pentagons (defined by the four pyrrole rings) or four hexagons (defined by the meso carbons, the two adjacent C–N groups, and the center of the porphyrin macrocycle). The diamagnetic shift $\Delta\delta$ (in ppm) of a proton i which is induced by one of these dipoles k is given by eq 3, where r_{ik} is the distance of the nucleus i from the center

$$\Delta\delta_{ik} = K_k(1 - 3\cos^2\theta_{ik})r_{ik}^{-3} \quad (3)$$

of the polygon k in angstroms and θ_{ik} is the angle between the vector r_{ik} and the normal to the polygon. Values of the constant were taken to be $K_h = 39.8$ Å^3 and $K_p = 28.0$ Å^3 for the hexagons and pentagons, respectively.[28] The contribution of the entire porphyrin macrocycle to the chemical shift of nucleus i is obtained by summing the contributions of the eight dipoles.

The ring currents of the four meso aromatic rings of the tetraarylporphyrins in the triads also contribute to the observed $\Delta\delta$ values. These contributions, which are relatively small, may be calculated by using the above equation with $K = 27.6$ Å^3.[28] Of course, such a calculation requires a knowledge of the orientation of the aryl rings relative to the porphyrin plane. These rings are not coplanar with the macrocycle for steric reasons.[29] As discussed previously,[28] we have assumed that these rings reside in two equally populated conformations at 45° angles with respect to the plane of the macrocycle.

It has been reported[27] that in certain cases, a double-dipole approximation which replaces each of the dipoles discussed above with two dipoles located one on either side of each polygon yields better results. We previously noted[28] that for carotenoporphyrin molecules, this double-dipole approximation yields essentially the same conformations as the single-dipole approximation but gives a poorer fit to the experimentally determined $\Delta\delta$ values. This is also true for the triads, and as a result, the single-dipole method has been used here.

(29) See, for example: Dirks, J. W.; Underwood, G.; Matheson, J. C.; Gust, D. *J. Org. Chem.* **1979**, *44*, 2551.

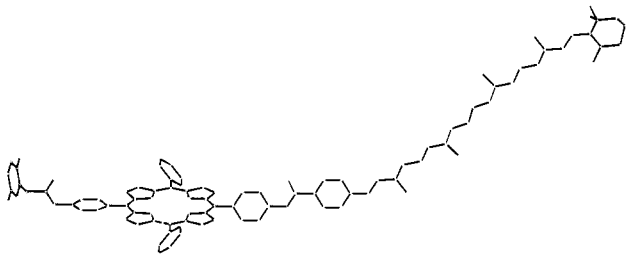

Figure 3. Time average solution conformation of triad **1**. Hydrogen atoms and methyl groups on porphyrin meso aryl rings are not shown.

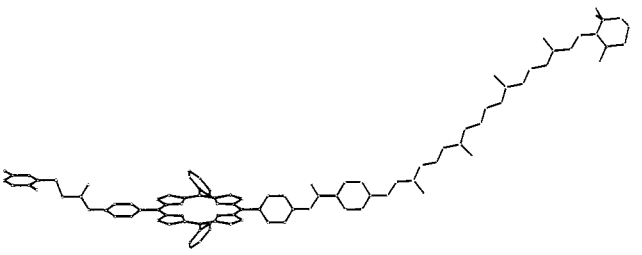

Figure 4. Time average solution conformation of triad **2**. Hydrogen atoms and methyl groups on porphyrin meso aryl rings are not shown.

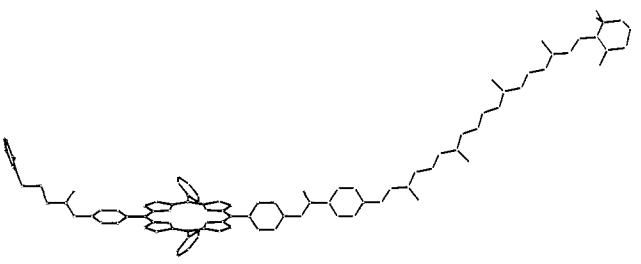

Figure 5. Time average solution conformation of triad **3**. Hydrogen atoms and methyl groups on porphyrin meso aryl rings are not shown.

Given the equivalent dipole model, one can begin to interpret the experimental $\Delta\delta$ values in terms of conformational information. The porphyrin macrocycle, the quinone ring, and the carotenoid system of conjugated double bonds are all expected to be relatively rigid structures. Most of the conformational mobility arises from the linkages joining these three moieties. Within these linkages, bond torsions are certainly of much lower energy than bond stretching or bending. Thus, the conformational analysis of the triads may be simplified by considering only conformational mobility about the dihedral angles in the linkages. The bond lengths, bond angles, and other dihedral angles are fixed at those values found for model compounds by X-ray diffraction studies. The numbering system used to identify these dihedral angles is shown in Figure 2.

The only carotenoid or quinone protons with significant $\Delta\delta$ values are those listed in Table III. The conformational analysis for each triad consisted of choosing an arbitrary starting conformation, calculating a $\Delta\delta$ value for each of the protons in Table III on the basis of the appropriate distances and angles for that conformation, determining the differences between the observed and calculated $\Delta\delta$ values, and then changing the dihedral angles as necessary and recalculating in order to minimize these differences. This type of iterative calculation is greatly facilitated by computerization, and we have therefore written computer programs which automatically carry out the procedure described above.[28]

The calculated $\Delta\delta$ values which best agree with the experimental values for all of the triads are reported in Table III. The corresponding dihedral angles are given in Table IV. The convention used for assigning dihedral angles is that they are measured

Table III. Observed[a] and Calculated[b] Chemical Shift Differences

	compound					
proton	**1**	**2**	**3**	**4**	**5**	**6**
C1′,5′	0.10	0.08	0.08	0.09	0.09	0.17
	(0.09)	(0.09)	(0.09)	(0.09)	(0.09)	(0.12)
C2′,4′	0.17	0.15	0.16	0.16	0.16	0.21
	(0.16)	(0.16)	(0.16)	(0.16)	(0.16)	(0.20)
C7′	0.07	0.06	0.06	0.06	0.06	0.10
	(0.06)	(0.06)	(0.06)	(0.06)	(0.06)	(0.07)
C8′	0.07	0.06	0.06	0.05	0.06	0.08
	(0.07	(0.07)	(0.07)	(0.07)	(0.07)	(0.09)
C19′	0.04	0.03	0.03	0.04	0.04	0.04
	(0.04)	(0.04)	(0.04)	(0.04)	(0.04)	(0.04)
C21						0.29
						(0.34)
Q3	0.20	0.12	0.09	0.08	0.13	0.19
	(0.20)	(0.14)	(0.09)	(0.07)	(0.14)	(0.20)
Q5	0.09	~0.03	0.04	0.03	0.04	0.09
	(0.07)	(0.07)	(0.03)	(0.04)	(0.07)	(0.07)
Q6	0.13	0.07	0.06	0.05	0.08	0.12
	(0.10)	(0.08)	(0.04)	(0.04)	(0.08)	(0.10)
Q7	0.38	0.18	0.15	0.11	0.20	0.37
	(0.34)	(0.21)	(0.15)	(0.09)	(0.21)	(0.34)
Q8		0.28	0.21	0.15	0.31	
		(0.35)	(0.21)	(0.15)	(0.35)	
Q9			0.30	0.23		
			(0.35)	(0.21)		
Q10				0.32		
				(0.32)		

[a] Observed $\Delta\delta = \delta_{triad} - \delta_{model}$ in ppm; data taken from Tables I and II. The model compounds were **45** and **50** for the carotenoid moieties and **57**, **59**, **60**, and **61** for the quinones, as discussed in the text. [b] Calculated differences in parentheses.

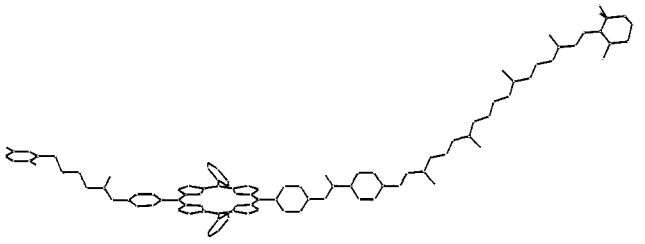

Figure 6. Time average solution conformation of triad **4**. Hydrogen atoms and methyl groups on porphyrin meso aryl rings are not shown.

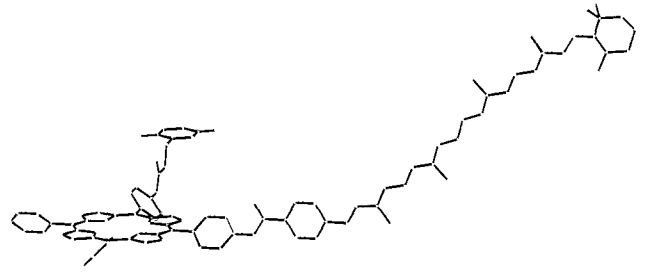

Figure 7. Time average solution conformation of triad **5**. Hydrogen atoms and methyl groups on porphyrin meso aryl rings are not shown.

clockwise when looking down the linkage bond from the end closest to the porphyrin macrocycle. The 0° conformation is that in which the bonds of the main linkage chain are eclipsed.

Figures 3–8 show the calculated conformations pictorially. In all cases, the quinone rings are at an angle of 90° with respect to the linkage chain. Although only one conformation is shown in the figures, there are actually two conformations, which differ only in the orientation of the quinone oxygen atoms. For the ring current calculations, these were assumed to be equally populated. A somewhat similar situation exists for the carotenoid, where two conformations differing by 180° at ϕ_{C5} (for **1–5**) or ϕ_{C6} (for **6**) might be expected. The differences in calculated $\Delta\delta$ values for the carotenoid protons in these two conformations are within the experimental error of the measured values. In addition, triad **1** features a 135° angle at ϕ_{Q4}. For the ring current calculations,

Table IV. Conformations of Carotenoporphyrin–Quinone Triads[a]

dihedral	compound					
angle	**1**	**2**	**3**	**4**	**5**	**6**
ϕ_{C1}	45	45	45	45	45	45
ϕ_{C2}	45	45	45	45	45	0
ϕ_{C3}	180	180	180	180	180	180
ϕ_{C4}	180	180	180	180	180	180
ϕ_{C5}	180	180	180	180	180	90
ϕ_{C6}						180
ϕ_{Q1}	45	45	45	45	45	45
ϕ_{Q2}	45	45	45	45	45	45
ϕ_{Q3}	180	180	180	180	180	180
ϕ_{Q4}	135	180	180	180	180	135
ϕ_{Q5}		180	180	180	180	
ϕ_{Q6}			180	180		
ϕ_{Q7}				180		
ϕ_{Q8}	90	90	90	90	90	90

[a] For numbering system, see Figure 3; for conventions for defining angles, see text. Angles are in degrees.

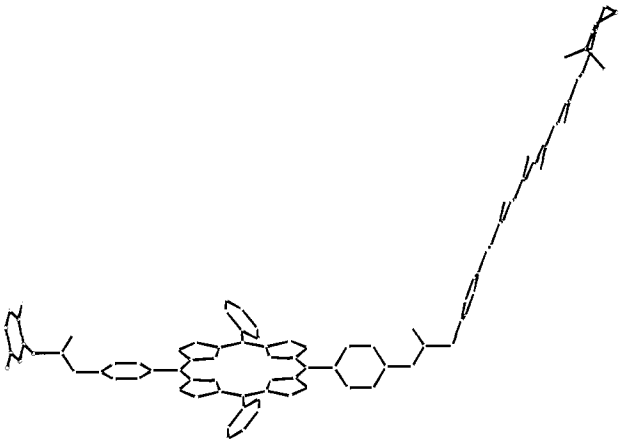

Figure 8. Time average solution conformation of triad **6**. Hydrogen atoms and methyl groups on porphyrin meso aryl rings are not shown.

the corresponding conformation with $\phi_{Q4} = 225°$ was considered to be equally populated. A similar conformational distribution was found for **6**.

In general, the agreement between observed and calculated $\Delta\delta$ values is quite good. The deviations which exist may be ascribed both to the approximations inherent in the mathematical model and to the choice of model compounds. The selection of model compounds is critical and yet unsatisfactory to some degree because one cannot eliminate the effects of the porphyrin ring currents without also eliminating the other electronic effects of the porphyrin macrocycle. For example, in the case of the carotenoid moiety, the model system chosen was the aniline amide of **17**, which includes the effect of the attached aryl ring, and this ring was therefore not considered in the ring current calculations. For triad **6**, which has a methylene group in the carotenoid linkage, an amide model was not available, and the methyl ester **45** was used instead. The methyl ester is not a particularly good model, and this undoubtedly explains the somewhat larger deviation between observed and calculated shift changes found for this molecule. In the case of the quinone moieties, only the simple amides were available as model systems. In all cases, the same conformations were calculated regardless of the choice of starting conformation or the minimization route. The possibility of false minima in the calculations may therefore be ruled out.

The calculations described above were all directed toward finding a single conformer, or a few closely related conformers, which best fit the experimental chemical shift data. This approach works well, as exemplified by the fact that for the series of triads **1–5**, the average deviation between the observed and calculated $\Delta\delta$ values is only 0.02 ppm. It will be noted that in the case of **2**, **3**, **4**, and **5**, the calculated conformer is the fully extended one with an anti conformation about each of the bonds joining the methylene groups. Although one would expect the all-anti con-

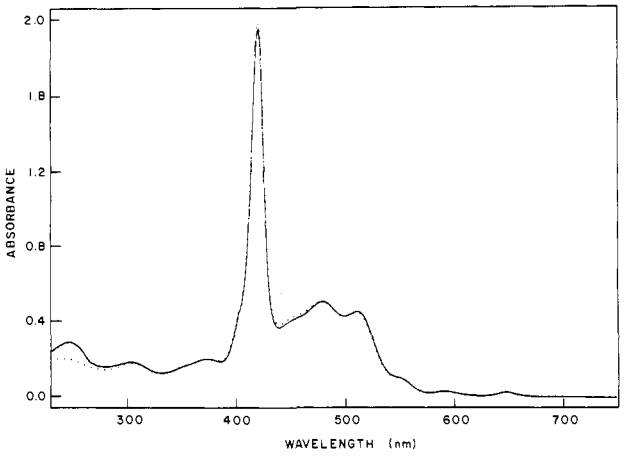

Figure 9. Absorption spectra of triad quinone **1** (—) and hydroquinone **21** (···) in dichloromethane solution.

former to be the most stable, one might also expect some of the gauche conformers to be populated. In order to investigate this possibility, theoretical $\Delta\delta$ values for the protons of the longest chain quinone (in triad **4**) were calculated assuming a weighted average of conformers with both anti and gauche stereochemistry about bonds ϕ_{Q5}–ϕ_{Q7} (Figure 2). Either 10% or 20% of the gauche rotamer about each of these bonds gave $\Delta\delta$ values which were essentially as good a fit to the experimental data as the all-anti conformation. Increasing the percentage of gauche rotamers to 30% or more gave errors which were unacceptably large for some protons. Physically, this means that too large a fraction of the nuclei were, on the average, too close to the porphyrin macrocycle in these cases.

Examination of the chemical shift values for the porphyrin–quinone systems **8–11** revealed that the shifts for the protons of the quinone moieties are virtually the same as those for the quinone portions of the corresponding triad molecules. Thus, the conformations of the quinone portions of **8–11** are essentially identical with those found in the triads. The dihedral angle values given in Table IV for the quinone linkages of the triads are therefore also valid for the porphyrin–quinones. In addition, the drawings of the solution time-averaged conformations of **1–4** also indicate the porphyrin–quinone relationships in **8–11**.

Absorption Spectra. The absorption spectra of triad quinone **1** and its hydroquinone precursor **21** are shown in Figure 9. Triad **1** has typical porphyrin absorption bands at 418 (Soret), 592, and 648 nm. Superimposed on these bands are carotenoid absorptions with maxima at 478 and 510 nm. These porphyrin and carotenoid bands are virtually unchanged from those in model carotenoids and porphyrins, and there is no evidence for strong interactions between the chromophores. Figure 9 also shows the quinone absorption at ca. 246 nm which is missing in the hydroquinone form. Careful comparison of the spectra of **1** and **21** in the 550–800-nm region provides no indication of porphyrin–quinone charge-transfer bands, within experimental error. The absorption spectra of **2–5** and **7** were virtually identical with that of **1**.

Fluorescence Decays. The results of the fluorescence lifetime measurements for triads **1–5**, porphyrin quinones **8–11**, and model compounds **12**, **14**, **18**, **21**, **35**, **62**, and **63** are reported in Table V. The four porphyrin models **12**, **14**, **35**, and **63** all yielded monoexponential decays with lifetimes of about 8 ns, which is approximately the fluorescence lifetime of tetra-*p*-tolylporphyrin itself. Thus, it is clear that attachment of the amino, amido, or hydroquinone functionalities to the porphyrin macrocycle has little effect on the fluorescence lifetime. The lifetime of **14** was not lengthened appreciably (<1 ns) after deoxygenating the sample with argon, and as a result the other samples were not deoxygenated.

The decay curves for **18**, **21**, and **62**, in which the porphyrin bears a carotenoid moiety, were best fit by the sum of two exponential decays. In each case, a minor, long-lived component was present to the extent of 3–4%. The amplitude of this component was sensitive to the degree of purification of the sample, and therefore most probably represents an impurity. The fluorescence lifetime of this impurity is, within experimental error, essentially that of an unperturbed porphyrin (see **12**, **14**, **35**, and **63**), and it is thus reasonable to ascribe this component to a small amount of material in which the carotenoid has been removed or destroyed.

Table V. Fluorescence Lifetimes (τ_i, ns) and Relative Amplitudes (RA, %) for Triads and Related Molecules in Dichloromethane[a]

compd	τ_1[b]	RA	τ_2	RA	X^2
1[c]	0.10	(96)	3.77	(3)	0.98
2	0.89	(99)	5.93	(1)	1.12
3	1.45	(98)	6.69	(2)	1.17
4	2.25	(95)	5.30	(5)	1.13
5	1.02	(98)	5.19	(2)	1.04
8[c]	0.10	(91)	7.25	(6)	1.15
9	1.16	(96)	8.58	(4)	1.15
10	1.45	(100)			1.13
11	2.97	(100)			0.98
21	3.36	(97)	9.76	(3)	1.03
62	3.54	(96)	9.57	(4)	1.13
18	3.37	(97))	8.91	(3)	1.20
63	8.27	(100)			1.16
35	7.70	(100)			1.16
14	8.13	(100)			1.13
12	7.73	(100)			1.23

[a] In many cases, these numbers represent the averages of several measurements carried out on several different spectrometers. [b] Typical limits of error on τ_1 are ±5%. [c] The results for this molecule were best fit as the sum of three exponentials. See text for discussion.

Table VI. Electron-Transfer Rate Constants and Intramolecular Distances

compd	k_{et}, s^{-1}	r_c, Å	r_{ee}, Å
1	97×10^8	12.8	4.8
2	8.3×10^8	14.9	6.2
3	3.9×10^8	15.3	7.4
4	1.5×10^8	17.2	8.7
5	6.9×10^8	14.9	6.2
8	99×10^8	12.8	4.8
9	7.4×10^8	14.9	6.2
10	5.6×10^8	15.3	7.4
11	2.0×10^8	17.2	8.7

In **18**, **21**, and **62**, the major component of the decay represents a reduction of the porphyrin fluorescence lifetime to ca. 3.4 ns. Thus, the linked carotenoid either opens a new pathway for decay of the porphyrin singlet state or enhances decay by one or more of the existing pathways. Similar quenching has been detected in other carotenoporphyrin molecules.[1-3] A possible explanation for this effect might be electron donation from the carotenoid to the porphyrin excited state to yield a short-lived charge-transfer state of the form $C^{\bullet+}$–$P^{\bullet-}$.[3] If this is indeed the correct explanation, the charge-separated state must return to the ground state very rapidly, as no carotenoid radical cation spectrum has been observed on the nanosecond time scale in these molecules.

The fluorescence of triad quinones **1–5** and porphyrin quinones **8–11** decays with a major, short-lived component and sometimes a minor (1–4%), longer lived contributor. The short lifetimes of the major components relative to those of model compounds may be attributed to electron transfer:

$$C\text{–}{}^1P\text{–}Q \rightarrow C\text{–}P^{\bullet+}\text{–}Q^{\bullet-}$$

which is step 2 of Scheme I. As mentioned above, the rate constant for this reaction may be calculated from eq 1 if the correct model compounds are used. For the triads **1–5**, the models chosen were **18**, **21**, and **62**, as the presence of the hydroquinone moiety has no apparent effect on the porphyrin fluorescence lifetime. For porphyrin–quinones **8**, **10**, and **11**, the model was **35**, whereas for **9**, model **63** was chosen. The electron-transfer rates, k_{et}, calculated from eq 1 are listed in Table VI.

The amplitude of the minor, longer lived component of the fluorescence decay of **2–5** and **9–11** depends upon the purification

procedure, and its lifetime is essentially that of the analogous species which lacks the quinone moiety. The most reasonable explanation for this component is that it is due to a small amount of impurity in which the quinone has been reduced to the hydroquinone. Even small amounts of reducing impurities in the solvent could account for the presence of this material at the very low concentrations used for the fluorescence lifetime work. In addition, the chromatographic purification process itself results in some reduction, which can be detected by the presence of the fluorescent hydroquinone-bearing porphyrin on the thin-layer chromatography plate. Due to the low amplitude of the long-lived component, both the calculated amplitude and lifetime of this component depend strongly on the particular data set and especially on the instrument response function. This fact probably accounts for the rather wide variation in lifetimes observed for this minor component. In the case of molecules **1** and **8**, the best fit of the experimental data included not only a major component with a lifetime of 100 ps and a minor component with a lifetime corresponding to that of the hydroquinone but also a small contribution (≤3%) from a third exponential decay with a lifetime of ca. 1 ns.

The fluorescence decay of **10** in dichloromethane was also studied as a function of temperature. The electron-transfer rate k_{et} decreased from 6.3×10^8 s^{-1} at 292 K to 1.2×10^8 s^{-1} at 187 K. A plot of ln (k_{et}/T) vs. $1/T$ for 10 temperatures yielded a straight line (correlation coefficient = 0.99), from which activation parameters $\Delta H^{\ddagger} = 1.3$ kcal/mol and $\Delta S^{\ddagger} = -14$ cal/deg-mol could be extracted (assuming $\kappa = 1.0$ in the Eyring equation).

Discussion

^{1}H NMR Studies. With regard to solution conformations, it is clear that all the triads have certain features in common. The carotenoid moieties are in identical conformations for **1–5** and are extended out away from the porphyrin ring rather than folded back over it. The carotenoid in **6** is also extended. The quinone side chains are similarly extended in all of the compounds, with anti conformations about the bonds in the methylene chains. Given these conformations for the side chains, there are in reality two possible conformations for the triad as a whole. The ones shown in the figures have the carotenoid and the quinone on the same side of the porphyrin plane. A second conformation, probably essentially equally populated, would have these two groups on opposite sides of the prophyrin plane.

Although Figures 3–8 are good representations of the gross aspects of the triad conformations, a word of caution is appropriate. Small changes in some of the dihedral angles yield structures with slightly different conformations which also fit the experimental data reasonably well. In addition, it must be remembered that the NMR calculations for **4** (and by extension for **2**, **3**, and the corresponding porphyrin–quinone species, which have similar $\Delta\delta$ values) are also consistent with a mixture of conformers having up to 20% gauche rotamers in the methylene chains. Thus, some conformational heterogeneity is possible, and indeed probable, in the systems with multiple methylene groups. Rotations about single bonds such as those in the porphyrin–quinone linkages of the triads are known to be facile. These facts have two consequences. In the first place, at any instant in time there will likely be very small populations of molecules with highly disfavored conformations, such as those in which the quinone is relatively close to the porphyrin macrocycle. The populations of these conformers will be too low to significantly affect the observed chemical shifts. Secondly, given enough time, a triad molecule in solution at ambient temperatures will eventually sample the energetically unfavorable conformations. These points are of significance for the interpretation of the photophysical studies of triads and similar molecules (see below).

The results obtained here demonstrate that analysis of porphyrin ring current induced shifts can yield valuable conformational information even in quite large and complex molecules. It should be remembered that the time-averaged solution conformations determined here cannot be treated in the same way as X-ray crystal structures for the reasons cited above. However, they are more suitable than crystal structures for the interpretation of photophysical measurements made in solution because the structure of a molecule in the solid state does not necessarily reflect its solution conformation. In addition, crystal structures cannot readily probe the possibility of intramolecular motion and conformational heterogeneity in solution, whereas the NMR approach can yield important information concerning these points.

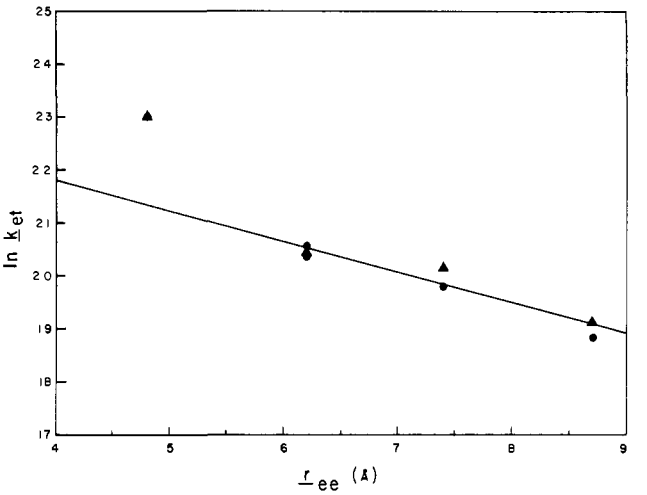

Figure 10. Plot of ln k_{et} (step 2 of Scheme I) vs. the distance from the edge of the porphyrin π-electron system to the edge of the quinone ring (Table VI). Circles represent carotenoporphyrin–quinone triads whereas triangles denote porphyrin–quinone species. The solid line is the least-squares fit for the seven compounds on the right-hand side of the plot.

Fluorescence Decay Studies. Most theories for nonadiabatic electron transfer predict[30-38] that for spherical donors and acceptors separated by a distance r, the electron-transfer rate constant k_{et} is given by

$$k_{et} = \nu \exp(-\alpha r) \quad (4)$$

The exponential factor approximates the distance dependence of the interaction between the wave functions for the electron on the donor and on the acceptor. The preexponential factor ν is a Franck–Condon term which includes the dependence of electron-transfer rates on the free energy change $(-\Delta G)$ for the reaction and on the differences between bond lengths and angles in the reactants and products, including their solvent shells. Although this theory was developed for small, rigid, spherical donors and acceptors rather than for large, asymmetric, conformationally mobile organic systems, it is instructive to discuss the results of the fluorescence decay measurements within this framework.

Donor–acceptor distance information is available from the results of the ^{1}H NMR studies discussed above and is listed in Table VI. The third column in this table gives the distance between the center of the porphyrin macrocycle and the center of the quinone aryl ring (r_{cc}) for each species. In these molecules, where the size of the donor and acceptor π-electron systems is large compared with the separation r, it would seem reasonable to employ an edge-to-edge distance of closest approach of the π-systems rather than a center-to-center distance, in eq 4. The

(30) Newton, M. D.; Sutin, N. *Annu. Rev. Phys. Chem.* **1984**, *35*, 437–480 and references cited therein.
(31) Boens, N.; De Brackeleire, M.; Huybrechts, J.; De Schryver, F. C. *Z. Phys. Chem. (Munich)* **1976**, *101*, 417–428.
(32) Newton, M. D. *Int. J. Quantum Chem., Quantum Chem. Symp.* **1980**, *14*, 363–391.
(33) Siders, P.; Cave, R. J.; Marcus, R. A. *J. Chem. Phys.* **1984**, *81*, 5613–5624.
(34) Kakitani, T.; Mataga, N. *J. Phys. Chem.* **1985**, *89*, 8–10.
(35) Van den Zegel, M.; Boens, N.; De Schryver, F. C. *Biophys. Chem.* **1984**, *20*, 333–345.
(36) Marcus, R. A.; Sutin, N. *Biochim. Biophys. Acta* **1985**, *811*, 265–322.
(37) Guarr, T.; McLendon, G. *Coord. Chem. Rev.* **1985**, *68*, 1–52.
(38) Devault, D. *Q. Rev. Biophys.* **1980**, *13*, 387–564.

edge of the quinone π-electron system can be approximated as the carbon atom bearing the methylene group which links the quinone to the rest of the molecule. In the case of the porphyrin, however, the choice is not so straightforward. Although the meso rings are not in the plane of the porphyrin macrocycle for steric reasons, neither are they at right angles to this plane,[29] and there must be some conjugation between these rings and the macrocycle. For this reason, we have chosen to define the edge of the porphyrin π-electron system as the carbon atom para to the point of attachment of the meso aryl ring to the porphyrin macrocycle. The resulting edge-to-edge distance (r_{ee}) is reported in the fourth column of Table VI. Other choices could clearly be made.

Equation 4 requires that a plot of ln k_{et} vs. r yield a straight line with a slope of $-\alpha$ and an intercept of ln ν. Figure 10 shows such a plot for triads **1–5** and porphyrin–quinones **8–11**. The distance parameter employed is the edge-to-edge separation r_{ee} as determined from ^{1}H NMR measurements in deuteriochloroform. Although the electron-transfer rates were measured in dichloromethane, the molecular conformations are expected to be similar in these two solvents.

It is apparent from the figure that although the data for compounds with two or more methylene groups (**2–5** and **9–11**) fall on a reasonably straight line, those for molecules with a single methylene spacer (**1** and **8**) deviate considerably from this line. There are several possible explanations for the deviation. In the first place, there is a difference in the free energy changes for the electron-transfer reactions of **1** and **8** relative to the other members of the series. The energy of the porphyrin first excited singlet state in C-^{1}P–Q is about 1.90 eV.[39] Cyclic voltammetric measurements of the redox potentials of **3**, **4**, and their porphyrin and quinone precursors in dichloromethane suggest that the energy of the C–P$^{\bullet+}$–Q$^{\bullet-}$ state is ca. 1.4 eV.[40] (The energy of the final C$^{\bullet+}$–P–Q$^{\bullet-}$ state is ca. 1.1 eV). Thus, the free energy change for step 2 in Scheme I is about 0.5 eV for these two molecules and their P–Q analogues. Comparison of our electrochemical results for the simple amide of the quinone moiety of **4** with those obtained by other workers for amides of the quinone in **1** and **8** which has only a single methylene spacer[41] reveals that the quinones with a single methylene group are better electron acceptors by ca. 0.14 eV in dichloromethane. Thus, the initial electron-transfer step for **1** and **8** is more exergonic than those for the other molecules by ca. 0.14 eV. For most systems, an increase in driving force translates into an enhancement in transfer rate in this range of free energy change. The degree of this enhancement depends upon the details of the Franck–Condon factors as mentioned above. However, if one examines recently published rate vs. $-\Delta G$ curves,[12u,34,42] it is clear that this free energy difference can account for deviations from linearity of the same order of magnitude as those observed for **1** and **8**.

There are other factors which may also contribute to the enhanced k_{et} for **1** and **8**. Coulombic stabilization of C–P$^{\bullet+}$–Q$^{\bullet-}$ due to the proximity of charges would be greater for **1** and **8** than for other members of the series, and such stabilization would lead to an increase in free energy change and therefore in rate. Through-bond contributions to the electron-transfer process[43,44] would be most important for these members of the series, as would any other breakdown of the postulated exponential decay of wave functions with distance.

Neglecting the points for **1** and **8** for the reasons outlined above, the remaining points on the graph in Figure 10 define a straight line within the experimental errors in k_{et} and r_{ee}. The slope of this line yields a value for α in eq 4 of 0.6 ± 0.07 Å^{-1} and the intercept a value for ν of $3 \pm 2 \times 10^{10}$. Although r_{ee} was chosen for the plot for the reasons discussed above, one may, of course, analyze the data by using other sets of distances. For example, a plot of ln k_{et} vs. r_{cc} from Table VI for **2–5** and **9–11** yields a straight line with essentially the same slope (α = 0.6 Å^{-1}) as was obtained for r_{ee} but with $\nu = 6.5 \times 10^{12}$.

Figure 10 shows that the data for **2–5** and **9–11** are consistent with the predicted exponential dependence of electron-transfer rate on distance within experimental error. In general, the value of the parameter α is a function of the particular system under study and is expected to vary from case to case. The value obtained for α in this study (ca. 0.6 Å^{-1}) is somewhat smaller than those obtained in many other systems; i.e., the distance dependence is relatively weak. For example, Hopfield and co-workers[45] have recently reported measurements of electron-transfer rate constants in two rigid porphyrin–quinone molecules in four different solvents. Although there is some uncertainty due to experimental constraints, a value of $\alpha \geq 1.4$ Å^{-1} may be estimated from their data. Miller and co-workers[46] have found α = 1.2 Å^{-1} for electron transfer between unlinked aromatic donors and acceptors in a rigid glass, as measured by pulse radiolysis techniques. In general, for a wide variety of systems, α is found to range from ca. 0.9 to 2.0 Å^{-1},[30,33,36] although values as low as 0.3 Å^{-1} have been reported.[36,47] It has also been noted that α often tends to be small for reactions involving excited states.[36]

One factor which may contribute to the relatively weak distance dependence of electron transfer observed with the triads is the effect of intramolecular motions and/or conformational heterogeneity. The distances in Table VI were calculated from time-averaged solution conformations based on NMR studies, which turn out to be the maximally extended ones (all anti in the methylene chains). That is, the porphyrin and the quinone are as far apart as possible, given the constraints of the linkage. In the case of **1** and **8**, electron transfer is rapid (ca. 10^{10} s^{-1}), and there are no degrees of rotational freedom in the linkage joining the porphyrin and the quinone that will affect the donor–acceptor separation significantly. In those systems with several methylene groups in the linkage such as **3**, **4**, **10**, and **11**, however, rotational freedom is much greater, and electron-transfer rates are slower by nearly 2 orders of magnitude. In these cases, some rotations about the single bonds in the linkages are likely during the lifetime of the excited singlet state.

In particular, internal rotations in the all-anti conformers of the molecules bearing several methylene groups in the P–Q linkage to yield conformations with one gauche arrangement might well occur on the time scale of electron transfer. The fact that the fluorescence decays for the molecules in question may be fit well by two exponentials, one of which may be ascribed to hydroquinone impurity, indicates either that only one conformation (or several with essentially equal P–Q separations) is present or that interconversion among the major conformers is rapid on the time scale of fluorescence. Thus, a molecule might sample several conformations during the excited singlet-state lifetime. Conformations in which the donor–acceptor separation is shortened would be expected to show enhanced electron-transfer rates, relative to the extended conformers. As a result, conformers which are not highly populated at the steady state (and hence do not contribute appreciably to the NMR time average measurement) may still make significant contributions to the observed electron-transfer rates and thus reduce the apparent α. In other words, because the calculated conformations from the NMR data are the most extended ones possible (largest r), any molecular motion during the lifetime of the excited singlet state can only decrease r from the calculated value, and this in turn would lead to an underestimation of α. Therefore, 0.6 may be a lower limit for the "true" value of α at the fixed donor–acceptor distances listed in Table VI.

(39) Seely, G. R. *Photochem. Photobiol.* **1978**, *27*, 639–654.
(40) We thank Doris Lexa of the Univetsité Pierre et Marie Curie (Paris VII) for performing these measurements.
(41) Wilford, J. H.; Archer, M. D.; Bolton, J. R.; Ho, T.-F.; Schmidt, J. A.; Weedon, A. C. *J. Phys. Chem.* **1985**, *89*, 5395–5398.
(42) Miller, J. R.; Calcaterra, L. T.; Closs, G. L. *J. Am. Chem. Soc.* **1984**, *106*, 3047–3049.
(43) Hush, N. S.; Paddon-Row, M. N.; Cotsaris, E.; Oevering, H.; Verhoeven, J. W.; Heppener, M. *Chem. Phys. Lett.* **1985**, *117*, 8 and references cited therein.
(44) Hush, N. S. *Coord. Chem. Rev.* **1985**, *64*, 135–157.
(45) Leland, B. A.; Joran, A. D.; Felker, P. M.; Hopfield, J. J.; Zewail, A. H.; Dervan, P. B. *J. Phys. Chem.* **1985**, *89*, 5571–5573.
(46) Miler, J. R.; Beitz, J. V.; Huddleston, R. K. *J. Am. Chem. Soc.* **1984**, *106*, 5057–5068.
(47) Milosavljevic, B. H.; Thomas, J. K. *J. Phys. Chem.* **1985**, *89*, 1830–1835.

Quantitative calculations suggest that this explanation is viable. Inspection of molecular models reveals that if one begins with the all-anti conformation in the P–Q linkage, only certain anti → gauche rotations lead to conformers in which the P–Q separation has been changed appreciably. These are 120° rotations about ϕ_{Q5} for **2**, **3**, **5**, **9**, and **10** and ϕ_{Q5} or ϕ_{Q7} for **4** and **11** (Figure 2). Although some combinations of these gauche and anti conformations lead to values of α which are little different from that found for the all-anti conformers, others give enhanced values of α. In an extreme case, a plot of ln k_{et} vs. r_{ee} for **2–5** and **9–11** assuming gauche conformations at ϕ_{Q5} for **3**, **4**, **10**, and **11** (but not for **2** and **9**) and anti arrangements elsewhere in the methylene chains yields α = 1.7 with a correlation coefficient of 0.95. Although this is not an especially likely combination of conformations, it does illustrate the principle involved.

It was noted above that the ^{1}H NMR data are compatible with an ensemble of conformers for the molecules having more than one methylene group in the P–Q linkage with up to 20% gauche conformations about the bonds joining methylene groups. Again, the fact that the fluorescence decay in these compounds can be fit with two exponentials, one of which is due to an impurity, suggests that in the case of such conformational heterogeneity, interconversion among the highly populated conformers must occur during the lifetime of the porphyrin excited singlet state, and the actual average distances over which electron transfer occurs will be less than those shown in Figure 10.

The above discussion has centered on the role of conformers with a single gauche bond in the methylene chain. In addition, large-scale folding motions of the polymethylene chain which would bring the quinone moiety several angstroms back toward the porphyrin (but not over it) are in principle possible for the molecules with three or four methylene groups. However, the time scale for such motions, which would involve at least two simultaneous gauche arrangements in the methylene chain, is expected to be slower than the time scale for electron transfer. For example, in carotenoporphyrins featuring a trimethylene linkage similar to (but not identical with) that in **3** and **10**, triplet energy transfer from the porphyrin to the carotene is mediated by such folding motions of the chain. This transfer occurs on the hundreds of nanoseconds time scale.[9] In addition, the temperature dependence for electron transfer measured for **10** argues against this type of folding back of the chain as the rate-determining step. The $\Delta H^{\ddagger}$ for electron transfer is 1.3 kcal/mol, whereas in polymethylene chains, a g^+g^- conformation such as that necessary for the folding back of the chain is generally taken to be ca. 3 kcal/mol above the all-anti state,[48] and the energy of activation for achieving this conformation should be even higher.

In this connection, it will be noted that interpretation of the temperature dependence for **10** by using the Eyring equation with the transmission coefficient κ = 1 leads to a fairly large negative entropy of activation of −14 cal/deg-mol. The data may be equally well accommodated by reducing κ, in accord with current theories for nonadiabatic electron transfer.[30,32-34,36-38]

Any participation by the σ-bonds of the linkage in the electron-transfer process would presumably enhance the rate and contribute to the observed distance dependence. Such "through bond" effects have been reported in other linked donor–acceptor systems.[43,44]

A primary goal of this work has been to identify the factors that control the energy, yield, and lifetime of charge-separated states which result from a two-step electron-transfer process such as that diagrammed in Scheme I. It is clear from the data presented above that increasing the separation between the porphyrin and the quinone decreases the rate of charge separation (step 2 in the scheme) and consequently decreases the yield of the initial C–P$^{\bullet+}$–Q$^{\bullet-}$ state. It must be realized, however, that such a decrease does not necessarily lead to a corresponding decrease in the yield of the final charge-separated state C$^{\bullet+}$–P–Q$^{\bullet-}$. The yield of the final state depends not only upon the rate of step 2 relative to those of the other pathways which deactivate the porphyrin singlet but also on the branching ratio of the back reaction (step 3) and the second electron-transfer step (step 4). In contrast to molecular systems with large values of α, the relatively weak dependence of electron-transfer rate on the number of methylene spacers in the triads should allow synthetic "fine tuning" of the rates of the various electron-transfer steps so as to maximize the yield and lifetime of the C$^{\bullet+}$–P–Q$^{\bullet-}$ state for different applications. As no fluorescence has been observed from C–P$^{\bullet+}$–Q$^{\bullet-}$ or C$^{\bullet+}$–P–Q$^{\bullet-}$, these questions must be investigated by using other spectroscopic techniques.

Acknowledgment. This work was supported in part by the National Science Foundation under Grants CHE-8209348, CHE-8515475, CHE-8409644, INT-821253, and INT-8514252 (CNRS-NSF exchance program), the North Atlantic Treaty Organization under Grant RG.083.81, and the CNRS under Grant 3064. Work at SERI was supported by the Division of Chemical Sciences, Office of Energy Research, U.S. Department of Energy. We thank Catherine Fenselau, Richard B. van Breemen, and the Middle Atlantic Mass Spectrometry Laboratory, a National Science Foundation shared instrument facility, for the FAB mass spectral studies.

Supplementary Material Available: Details of the synthesis of the compounds discussed in this paper (32 pages). Ordering information is given on any current masthead.

(48) Flory, P. J. In *Statistical Mechanics of Chain Molecules*; Wiley-Interscience: New York, 1969; p 139.